Master's Thesis

Seasonal evolution of the permanent pycnocline at Maud Rise, Weddell Sea, Antarctic

M.Sc. Ocean and Climate Physics

Institute of Oceanography

Faculty of Mathematics, Informatics and Natural Sciences

Universität Hamburg

Viktoria Nikolaus

Enrollment number: 7166315

First Supervisor:

Prof. Dr. Eleanor Frajka-Williams

Second Supervisor:

Prof. Dr. Alberto Naveira Garabato

April, 2024

Seasonal evolution of the permanent pycnocline at Maud Rise, Weddell Sea, Antarctic

Abstract

Understanding the seasonal dynamics of the permanent pycnocline is crucial for explaining the physical processes governing oceanic stratification and its implications for ocean dynamics. This study investigates the seasonal evolution of the permanent pycnocline at Maud Rise, a key region in the Southern Ocean characterised by sea-ice variability and the occurrence of polynyas. Utilising data from two Argo floats, one during a polynya year and another one during a non-polynya year, to analyse the temporal variability of the permanent pycnocline's depth and strength. The results reveal strong seasonal variability in the characteristics of the permanent pycnocline at Maud Rise, driven by the interplay between freshwater and temperature forcing, as well as wind stress. At the beginning of the year, the permanent pycnocline shoals until it merges with the seasonal pycnocline and its strength increases. In winter, cooling and sea-ice formation deepen and weaken the pycnocline, destabilising the upper ocean. Additionally, the polynya year and inter-annual variability in upper ocean freshwater content show the influence of a strong gradient between the upper ocean and warmer, saltier, deeper water masses. Wind stress also

Overall, this study provides valuable insights into the seasonal evolution of the permanent pycnocline in a key region of the Southern Ocean, advancing our understanding of the underlying mechanisms.

Contents

List of Figures

1 Introduction

The Southern Ocean's permanent pycnocline is a layer of elevated stratification that plays a fundamental role in organising the global overturning circulation (DeVries and Primeau, 2011). It acts as a barrier between the upper mixed layer and the slowly ventilated deeper ocean (Gnanadesikan, 1999). The ocean's mixed layer and permanent pycnocline play a crucial role in determining the ocean's impact on the world's climate by absorbing heat and carbon from transformed water masses (Abernathey et al., 2016; DeVries and Primeau, 2011; Pellichero et al., 2017). Understanding the seasonal evolution of this highly stratified layer is a first step to unravelling the dynamics of the Southern Ocean that influence the permanent pycnocline. The upper ocean's properties and stability are affected by multiple processes such as air-sea fluxes, air-sea stress, lateral advection, vertical entrainment and ice-ocean fluxes (Pellichero et al., 2017). As Southern Ocean sea ice exhibits one of the strongest seasonal cycles on Earth (Handcock and Raphael, 2020), it impacts the upper ocean through processes associated with sea-ice formation and melt.

Classic pycnocline theory focuses on temperature gradients to determine vertical stratification (Carmack, 2007). This theory is based on the premise that temperature gradients are the primary factor influencing vertical stratification. This is reasoned by the fact that changes in buoyancy in the ice-free ocean are governed by temperature (Pellichero et al., 2017). This theory proposes two distinct regimes for the formation of pycnoclines. The adiabatic regime, which is characterised by the remapping of surface density gradients of the subtropical gyres explains the formation of the seasonal pycnocline. These gradients were formed by thermal atmospheric forcing and then transported to the interior of the ocean by Ekman downwelling (Luyten et al., 1983). The second regime explains the formation of the permanent pycnocline through a diabatic process, driven by an advection-diffusion balance. There temperature gradients of the subpolar oceans are remapped onto the vertical dimension(Samelson and Vallis, 1997). However, due to the sea-ice cycle, the stratification and stability of the polar, ice-covered oceans are influenced by a combination of heat and freshwater fluxes(Martinson and Iannuzzi, 1998). In the ice-covered polar oceans, freshwater fluxes in the form of brine released during sea-ice formation and freshwater input due to sea-ice melt have been shown to influence the density stratification and buoyancy significantly more compared to heat fluxes(Abernathey et al., 2016; Pellichero et al., 2018). In addition to changing the underlying density structure and stability, sea ice affects the heat flux between air and ocean due to its insulating properties (Martinson and Iannuzzi, 1998). Another reason why the influence of freshwater fluxes on the density structure of the upper ocean is greater is that the thermal

expansion coefficient of seawater near freezing temperatures is close to zero. Therefore, heat fluxes have a lower impact on density than freshwater fluxes. In addition, the stratification in the Southern Ocean cannot be explained by remapping horizontal density gradients but rather by the density gradient at the base of the mixed layer in winter(Klocker et al., 2022).

Given the importance of sea-ice formation and melt on density, salinity should not be neglected when analysing the development of the permanent pycnocline in the Southern Ocean, as is frequently the case in classical pycnocline theories. The seasonal cycle of sea ice plays a pivotal role in shaping the vertical stratification and thus the stability of the upper ocean, the evolution of the pycnocline and the ventilation of deep water (Klocker et al., 2022; Martinson and Iannuzzi, 1998). The cycle described above has significant implications for the formation and transformation of deep ocean water masses, especially in weakly stratified regions such as the Weddell Sea (Gordon, 1991). The process of deep water formation, which is crucial to the global oceanic circulation system, is significantly influenced by the seasonal variability of sea ice in this area. In the Weddell Sea, the water column is particularly weakly stratified with the permanent pycnocline at 100 m depth(Libera et al., 2022). This weak stratification makes the Weddell Sea prone to deep convection, particularly in the context of brine rejection during sea-ice growth. Despite this weak stratification, the permanent pycnocline is rarely eroded throughout the winter, even though only a small addition of brine would erode the pycnocline. This erosion would then lead to deep convection. These deep convection events do occur in the Weddell Sea, ableit only rarely (Martinson and Iannuzzi, 1998; Wilson et al., 2019). The persistence of the permanent pycnocline throughout the year can largely be explained by negative feedback to ice growth due to entrainment of warm circumpolar deep water (CDW) from below the permanent pycnocline (Wilson et al., 2019)(Martinson, 1990). This convection is a crucial process in the formation of the world's deep waters, with significant implications for the global climate (Gordon, 1991).
Maud Rise is a seamount located in the Weddell Sea, approximately 700 km north of the Antarctic continent. The site is prone to deep convection and erosion of the permanent pycnocline. Maud Rise rises from a depth of about 5000 m to less than 1700 m below the ocean's surface at its shallowest point. Its diameter is in the order of 100km and it is situated at 65 °S and 2.3 °E (Beckmann et al., 2001). The seamount stands in the way of CDW being advected into the Weddell Gyre; due to the conservation of potential vorticity, the flow has to circumvent Maud Rise and thereby creates a Taylor column on top of the seamount. The water on top is distinguished by a cold water Taylor cap and warmer water flanks around the

seamount (Muench et al., 2001) with jets of warm water at the northern and north-western flank (Brandt et al., 2011). As a result of these dynamics, Maud Rise is known for its reduced sea-ice cover, early onset of sea-ice melt and open ocean polynyas. (De Steur et al., 2007). A polynya is a large opening in the sea-ice cover, enabling an air-sea exchange even during periods when the ocean is normally covered by sea ice, leading to modification of ocean properties. The largest known occurrence of such a polynya in the Weddell Sea was during the winters of 1974 to 1976. The formation of the polynya began in the Maud Rise region and developed westwards into the centre of the Weddell Sea. Smaller polynyas have more recently been observed at Maud Rise in 2016 and 2017. The surface buoyancy loss associated with polynyas can lead to deep convection (Martinson, 1990) and have further climatic implications in terms of ocean circulation(Pedro et al., 2016) and carbon sequestration (Resplandy et al., 2015).

Nonetheless, as previously described, sea-ice growth is also limited by heat flux from below the pycnocline, which is entrained during mixed layer deepening (Martinson, 1990). Thus, not only do freshwater fluxes influence the permanent pycnocline, but rather a combination of the seasonal sea-ice cycle and buoyancy fluxes.

The pycnocline in the Southern Ocean is thought to be formed as a result of mixing during continuous sea-ice melt throughout the year (Klocker et al., 2022) instead of outcropping isopycnals. However, it is not entirely clear which processes influence the properties of the pycnocline. My aim is to analyse the seasonal evolution of the permanent pycnocline and to determine which aspect might affect it.

Despite the importance of the Southern Ocean's permanent pycnocline with regard to the global overturning circulation, the processes affecting the pycnocline are poorly understood. This can partly be explained by the scarcity of observational data in the Southern Ocean, especially during sea-ice-covered periods. The scarcity of observational data in the Southern Ocean remains a challenge to understanding its dynamics. Argo floats, specifically, Polar Argo floats, that have an ice avoidance mechanism enabled us to obtain data even during austral winter for sea-ice regions (Klatt et al., 2007). This thesis utilises measurements from two Argo floats that appear to be trapped in the Taylor Column above Maud Rise: one during a non-polynya year, 2019, and another during a polynya year, 2016. In addition, I use passive microwave sea-ice concentration data to analyse the timing and concentration of sea ice in relation to oceanic variables. To analyse the impact of wind on the upper ocean I use wind stress data from an atmospheric reanalysis.

Furthermore, I compare my findings from the analysis of these two years and floats with the Biogeochemical - Southern Ocean State Estimate (SOSE) iteration 105, an ocean data assimilation between 2008 and 2012.
This thesis starts with a detailed description of the data and methods used, followed by an analysis of the upper ocean properties measured by the Argo floats and the SOSE. This is followed by a description of the seasonal changes in upper ocean heat content and freshwater anomaly to quantify the visually observed changes. Further, the influence of wind stress on the upper ocean properties in the Argo 2019 and SOSE data are analysed. Then the findings from the first part are compared to the results of the analysis for the 2016 Argo float. After that follows the discussion of the results, as well as a conclusion and an outlook on further research.

2 Data and Methods

2.1 Data

2.1.1 Argo floats

Measurements from two Argo floats that appeared to be trapped in the Taylor column above Maud Rise are used. For 2016, float 5904471 and for 2019 float 5905382. The Argo floats did not follow the same trajectories but remained close to or above the plateau of Maud Rise (Fig. 1). The Argo floats are programmed to measure profiles every 10 days from a depth of about 2000 m to the surface with depth intervals of about 2 dbar. The selection of floats was based on their location at the plateau of Maud Rise, their completion of a full annual cycle and their "good" quality flags (QC=1). The region of Maud Rise region is defined as the area between $62^oS - 68^oS; 0^oE - 10^oE$. The data is available at https://dataselection.euro-argo.eu/. Out of the data from both floats, I used adjusted variables: 'PRESSURE ADJUSTED', 'TEMP ADJUSTED' and 'PSAL ADJUSTED', as well as 'Date', 'Latitude' and 'Longitude'. The adjusted variables are pre-processed to remove known biases, such as sensor drift. The Argo float CTD measures with an accuracy of 0.001 psu for salinity, 0.1 dbar for pressure and 0.001 °C for temperature (Argo, nd). The data are limited to the upper 300m of the ocean to analyse upper ocean processes. No position or data can be transmitted while the Argo float is under the sea ice. The Argo float stores the measurements until it resurfaces and can transmit data again (Klatt et al., 2007). The positions of the individual profiles under sea ice are linearly interpolated between the last and first surfacing of the float(Wong and Riser, 2011).

Argo float 2019

The 5905382 Argo float was located at the southernmost point of the Maud Rise plateau at the beginning of 2019. It subsequently drifted westward and then northward. The last known GPS location was recorded at the end of May. Subsequent interpolation to the next known location in mid-December suggests an eastward and slightly southern drift. Despite the data collection schedule, which was programmed to take measurements every 10 days, there are gaps in the data for March and May (Fig. 4). During these months, only one profile was measured each month.

Argo float 2016

In 2016, the Argo float was located primarily in the centre of Maud Rise. It commenced the drift south of the seamount's shallowest point, in close proximity to the location where the Argo float from 2019 was located in March. The Argo float 5904471 remained under sea ice until mid-January. The Argo float subsequently moved northwards towards the centre of Maud Rise until mid-June, at which point the last known GPS location was registered prior to the onset of the sea-ice season. The interpolated location indicates a southward drift across the shallowest point where the float resurfaced at the end of December.

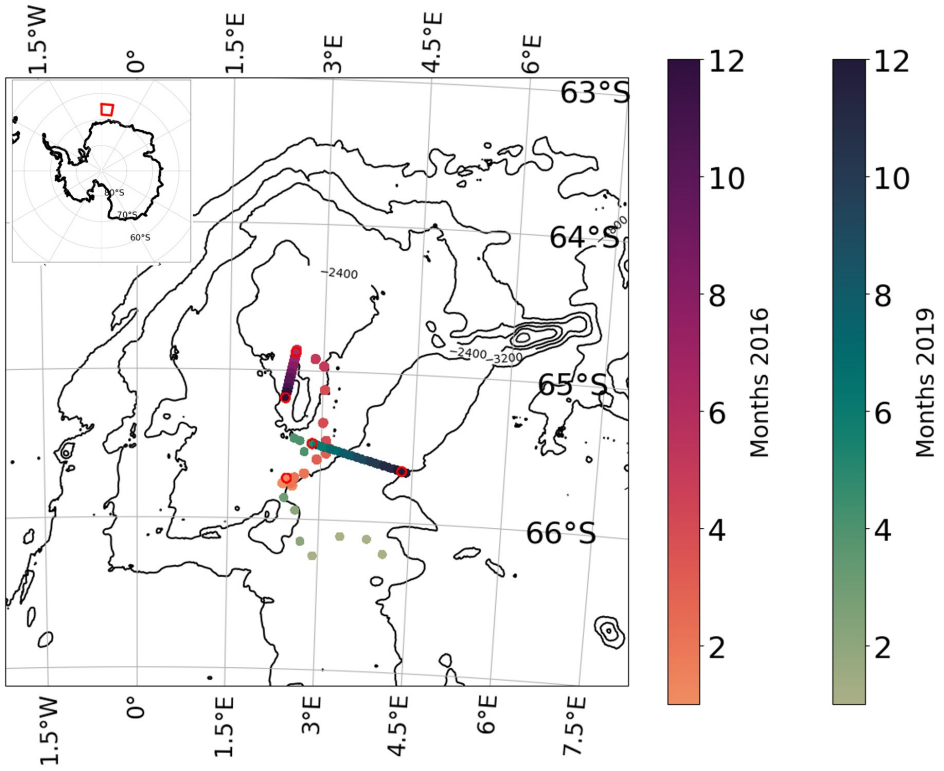

Figure 1: Trajectories of both Argo floats on top of the bathymetry of Maud Rise. The colour bars indicate the months of the individual years. In pink for 2016 and green for 2019. The red circles around some individual dots show when the floats surfaced last or resurfaced for the first time. The inlay in the upper left-hand corner of the figure depicts a map of Antarctica, with the red box showing the region of Maud Rise, which is located between 62°S − 68°S and 0°E − 10°E.

2.1.2 Biogeochemical Southern Ocean State Estimate

The Biogeochemical Southern Ocean State Estimate (SOSE) (Scripps Institution of Oceanography, 2016) is the successor of the Southern Ocean State Estimate. The estimate is an observation-constrained numerical ocean model. The assimilated observational datasets include satellite altimetry, in-situ temperature and salinity profiles from BCG-Argo floats, as well as measurements obtained during oceanographic campaigns. The model employs the Massachusetts Institute of Technology general circulation model (MITgcm), which has been configured for the Southern Ocean domain. The estimate has a horizontal resolution of 1/3° and 52 vertical layers. The spacing of the vertical layers varies with depth from 4.2 m at the surface to 21 m at 300 m. The output is available at three-day intervals from 2008 to 2012 (Verdy and Mazloff, 2017). For the purpose of this analysis, the following variables were used from iteration 105: 'potential temperature', 'salinity', 'zonal surface wind stress', 'meridional surface wind stress' and 'sea ice fractional ice-covered area'.

2.1.3 Ancillary data

Sea-ice concentration

The daily sea-ice concentration (SIC) data used in this study is obtained from a passive microwave satellite for the years 2016 and 2019. This data is provided by EUMETSAT Ocean and Sea Ice Satellite Application Facility (OSISAF) (Copernicus Climate Change Service (C3S), 2020) in a resolution of 25 km × 25 km. The SIC is average over the Maud Rise region, as previously defined as $62^{o}\mathrm{S} - 68^{o}\mathrm{S}; 0^{o}\mathrm{E} - 10^{o}\mathrm{E}$. The product's target accuracy lies at 15% (EUMETSAT Ocean and Sea Ice Satellite Application Facility, 2023). The maximum and minimum values observed for each day represent the uncertainty associated with the actual SIC above the float.

Wind stress

The eastward and northward turbulent surface stress, which is available 4x daily, from the NCEP-NCAR Reanalysis I provided by NOAA (Kalnay et al., 1996), are used in this thesis. The data are available on a $2.5^{\,o} \times 2.5^{\,o}$grid. Only data points in the previously defined Maud Rise region are considered.

2.2 Methods

Hydrographic data

The Argo float data was linearly interpolated on a regular vertical grid using the GliderTools Python package grid function to 2 m bins (Gregor et al., 2019). The GSW Oceanic Toolbox was employed to calculate additional variables, including but not limited to absolute salinity, conservative temperature, and density (McDougall and Barker, 2011). The mixed layer depth (MLD) is calculated using the GliderTools package (Gregor et al., 2019) with a density threshold of $0.01\,\mathrm{kg\,m^{-3}}$. In order to determine the vertical stratification of the ocean, the Brunt-Vaisälä frequency (N^2)is calculated using the Python package: The Gibbs SeaWater (GSW) Oceanographic Toolbox of TEOS-10 (McDougall and Barker, 2011). The equation used in the package is as follows:

$$N^2 = -\frac{g}{\rho}\frac{\partial \rho(z)}{\partial z} \tag{1}$$

N^2 gives a measurement of the ocean's stability. Lower values of N^2 indicate that less energy is required for mixing the water column, while higher values indicate a stable water column (Gill, 1982). Rather than defining the permanent pycnocline as the second peak in N^2 I follow Libera et al. (2022); the permanent pycnocline is defined as the maximum of the vertical temperature gradient dT/dz. This definition is supported by the observation that the temperature inversion

occurs at the depth of the permanent pycnocline and the second maximum in dS/dz and $\mathbf{N^2}$ (Fig.2). The first maximum is not only computationally more straightforward to identify, but since the seasonal and permanent pycnocline merge, the double peak feature in dS/dz and N^2 vanishes during winter, allowing for the identification of a single peak.

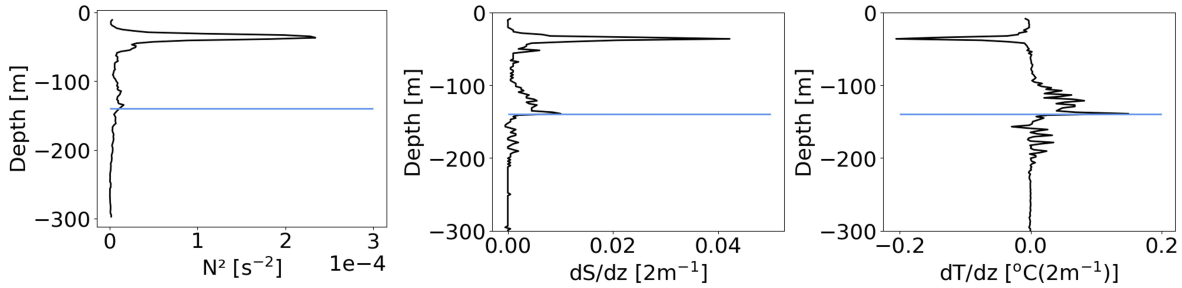

Figure 2: Example profiles from January 2019 of N^2, dS/dz and dT/dz

Freshwater anomaly

As another measure of upper ocean stability,the freshwater anomaly (FWA) is calculated using the adjusted salt deficit (SD*) as introduced in Wilson et al. (2019). This approach is based on the salt deficit as defined by Martinson (1990). This measure is more robust compared to N^2. The integrated freshwater anomaly of the mixed layer and the halocline calculates the meters of sea-ice growth needed to erode the entire halocline and thereby permit convection (Wilson et al., 2019).

$$\mathrm{FWA} = \frac{1}{\Delta \mathrm{S_i}} \int_0^{250} [\mathrm{S}(250) - \mathrm{S}(\mathrm{z})] \mathrm{dz} \tag{2}$$

With $\Delta \mathrm{S_i} = 30$psu (Martinson and Iannuzzi, 1998) being the difference between sea-ice salinity (4 psu) and MLD salinity (34 psu). I integrated the depth range from $0 - 250\,\mathrm{m}$, as this encompasses the permanent pycnocline throughout all seasons and years. A larger value indicates that more additional sea-ice growth is necessary, to entrain the halocline, while smaller values indicate a less stable upper ocean.

Ocean heat content

I calculated the integrated upper ocean heat content (OHC):

$$\mathrm{OHC} = \int_0^{250} \rho \, \mathrm{c_p} \, \mathrm{T(z)} \, \mathrm{dz} \tag{3}$$

The specific heat capacity, c_p, was calculated for each profile and depth using the GSW Oceanic Toolbox functions (McDougall and Barker, 2011). ρ_0 is the reference density of seawater $\rho_0 = 1027.2\,\mathrm{kg\,m^{-3}}$. Integration was performed over the upper ocean layer $0 - 250\,\mathrm{m}$ and across the depth of the winter permanent pycnocline, $100 - 200\,\mathrm{m}$.

$$\mathrm{OHC_P} = \int_{100}^{200} \rho \, \mathrm{c_p} \, \mathrm{T(z)} \, \mathrm{dz} \tag{4}$$

As previously stated, the water column remains stable during brine input due to a basal heat flux that prevents further sea-ice growth. The objective is to identify the source of a change in OHC by examining the changes in overall OHC and across the pycnocline (OHC_P).

Wind stress curl and upwelling

To calculate wind stress curl from the x- and y- components of wind stress the following equation is used:

$$\nabla \times \tau = \frac{\partial \tau_y}{\partial x} - \frac{\partial \tau_x}{\partial y} \tag{5}$$

The goal is to determine upwelling. Consequently, in order to calculate, it is first necessary to determine the vertical Ekman velocity is needed. This velocity, expressed in meters per second, is derived from the wind stress curl following this equation:

$$\mathrm{w_E} = -\frac{1}{\rho_0 \mathrm{f}} \cdot \mathrm{k} \cdot \nabla \times \tau \tag{6}$$

With k being the vertical unit vector ρ_0 is the reference density of seawater $\rho = 1027.2\,\mathrm{kg\,m^{-3}}$ and f the Coriolis parameter for 65° S. Integrating the upwelling velocity over time gives the Ekman displacement.

$$\text{Ekman Displacement} = \int_{\mathrm{t_0}}^{\mathrm{t_f}} \mathrm{w_E(t)}\,\mathrm{dt} \tag{7}$$

with t_0 being the initial time step of the measurement period and $\mathrm{t_f}$ the final time step, dt is the available timestep of the data. To obtain a rolling average for both wind stress curl and Ekman displacement, xarray's rolling function was used to create rolling averages for a 30-day window (Hoyer and Hamman, 2017).

3 Results

3.1 Seasonal changes of the upper ocean and permanent pycnocline characteristics

The seasonal evolution of upper-ocean salinity and temperature exhibits a distinct annual cycle. The 2019 Argo float and SOSE data show a fresh and warm mixed layer in January. The seasonal pycnocline separates the mixed layer from the remnants of the so-called Winter Water (WW) formed in the previous year and is saltier and colder at a depth of about 50 m (Fig. 4.1 and Fig.4.2). However, beneath this stable temperature stratification lies a temperature inversion: the slowly renewing warm and salty Circumpolar Deep Water (CDW) lies underneath the cold and fresher WW at around 170 m in 2019. The strong gradient in salinity stabilises the water column and prevents or dampens mixing. Until May, the mixed layer cools and sea ice begins to form, resulting in a deepening of the mixed layer and the formation of WW. In May, the mixed layer deepens to a depth of about 100 m in 2019. In austral winter, the mixed layer continues to deepen and the salinity increases from 34.34 in January to 34.68 in October. From June onwards, the mixed layer temperature remains close to the freezing point of $-1.8\,^{\circ}$C. After October, the mixed layer freshens to 34.16 by the end of December, due to freshwater input caused by sea-ice melt. This leads to stronger gradients in salinity and changes in the water column's stability, and the seasonal pycnocline separates from the permanent pycnocline. The seasonal cycle of temperature and salinity exhibits a consistent pattern of cooling and salinification, followed by warming and freshening, across years in the SOSE. However, the absolute values differ between the years: the warming at the beginning of each year is more pronounced in 2008 and 2011 (Fig. 4.1.a), while the temperature gradient between the upper ocean and the warm CDW decreases at the end of the time period. Similarly, salinity also differs between the years: The winter mixed layer became increasingly fresher over the course of the time series, reaching a minimum value in 2011. The average salinity of the mixed layer over the winter months (June to September) decreased from 34.38 ± 0.03 in 2008 to 34.25 ± 0.03 in 2011.

The seasonality in salinity and temperature is reflected in N^2 and the permanent pycnocline (Fig. 4.3). At the beginning of the year, the first maximum of N^2 is located at the barrier between the mixed layer and the WW, shallower than 50 m. The second gradient in salinity and temperature at a depth of 170 m, that separates WW and CDW, leads to a second maximum in N^2. This depth also coincides with the maximum of dT/dz and represents the permanent pycnocline, as explained in the methods section, at a depth below 150 m. During the mixed

layer deepening, the permanent pycnocline shoals until it merges with the seasonal pycnocline in May at a depth between $90 - 100\,\mathrm{m}$. This merging of the seasonal and permanent pycnocline results in a singular peak in N^2. The pycnocline continues to deepen until mid-August and remains at a rather constant depth of 150 m during the remainder of winter. In particular, the strong seasonal pycnocline at the beginning of the year shields the ocean below from mixing associated with air-sea interactions. Until winter at the start of the sea-ice formation, the seasonal pycnocline deepens due to densification and the lower oceanic layer is more vulnerable to exchange across the permanent pycnocline. The strength of the permanent pycnocline also displays a slight seasonal cycle. Upon merging with the seasonal pycnocline, the permanent one strengthens. In winter, the strength weakens continuously until the end of the year (Fig. 3.b).

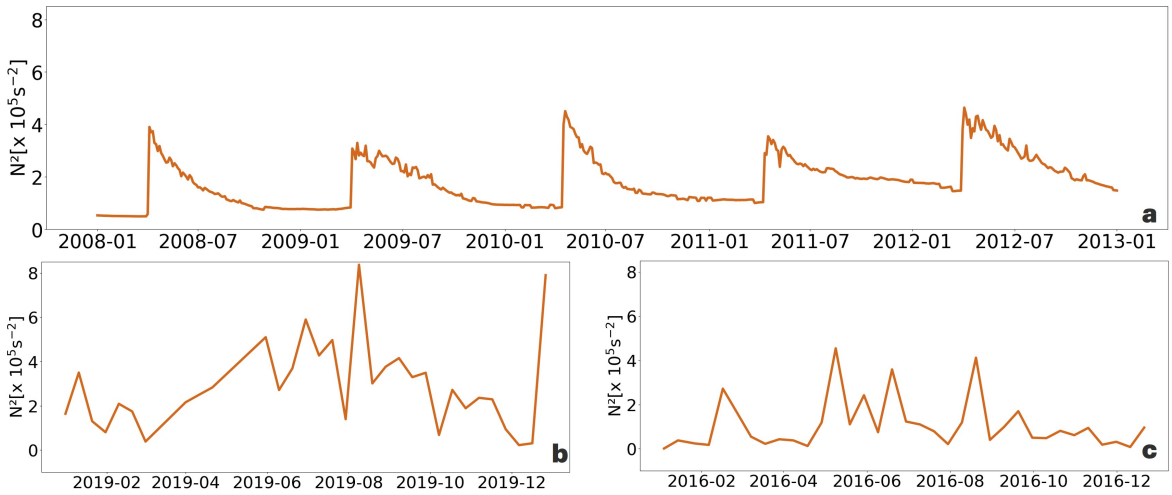

Figure 3: Evolution of N^2 at the depth of the permanent pycnocline. a) SOSE data, b) 590538 Argo float in 2019 c) Argo float 5904471 in 2016

In the SOSE, the shoaling of the permanent pycnocline is rather steep and to a shallower level compared to the Argo 2019 data. In addition, the temperature range in which the maximum of $\mathrm{d}T/\mathrm{d}z$ resides is colder in the SOSE at $-0.90^{\circ}\mathrm{C} \pm 0.26^{\circ}\mathrm{C}$ compared to $-0.78^{\circ}\mathrm{C} \pm 0.46^{\circ}\mathrm{C}$ in 2019. However, both lie within the standard deviation of the other. The timing of the mixed layer deepening roughly agrees between the SOSE and 2019. In the SOSE, the deepening commences in the second half of March, while the deepening starts in 2019 at the beginning of April. The timing of the convergence of seasonal and permanent pycnoclines has a similar time difference. For the SOSE, the pycnoclines merge during April, while in 2019 in May. The following deepening during winter lasts for both throughout winter until the maximum is reached at the end of August or at the beginning of September. The observed time lag could also be attributed to the coarser vertical resolution in the SOSE, some processes might not

be resolved as detailed. Even though the cycle roughly agrees throughout all the years, the permanent pycnocline in the SOSE is shallower towards the end of the data series. In 2012, it is closer to 100 m than 150 m like it was in 2008. The strength of the permanent pycnocline shows the same seasonal cycle as in 2019 — a strong increase upon merging with the seasonal pycnocline and the following decrease (Fig. 3). The strength (Fig.3) and depth (Fig. 4.3) of the permanent pycnocline remain constant after August until both pycnoclines merge in the next year. The absolute magnitudes are lower compared to 2019. The maxima for the SOSE data coincide with the lower values of N^2 in 2019. The hydrographic data show a seasonal cycle in the strength and position of the permanent pycnocline. This cycle follows changes in temperature and salinity and associated changes in the vertical displacement of the mixed layer.

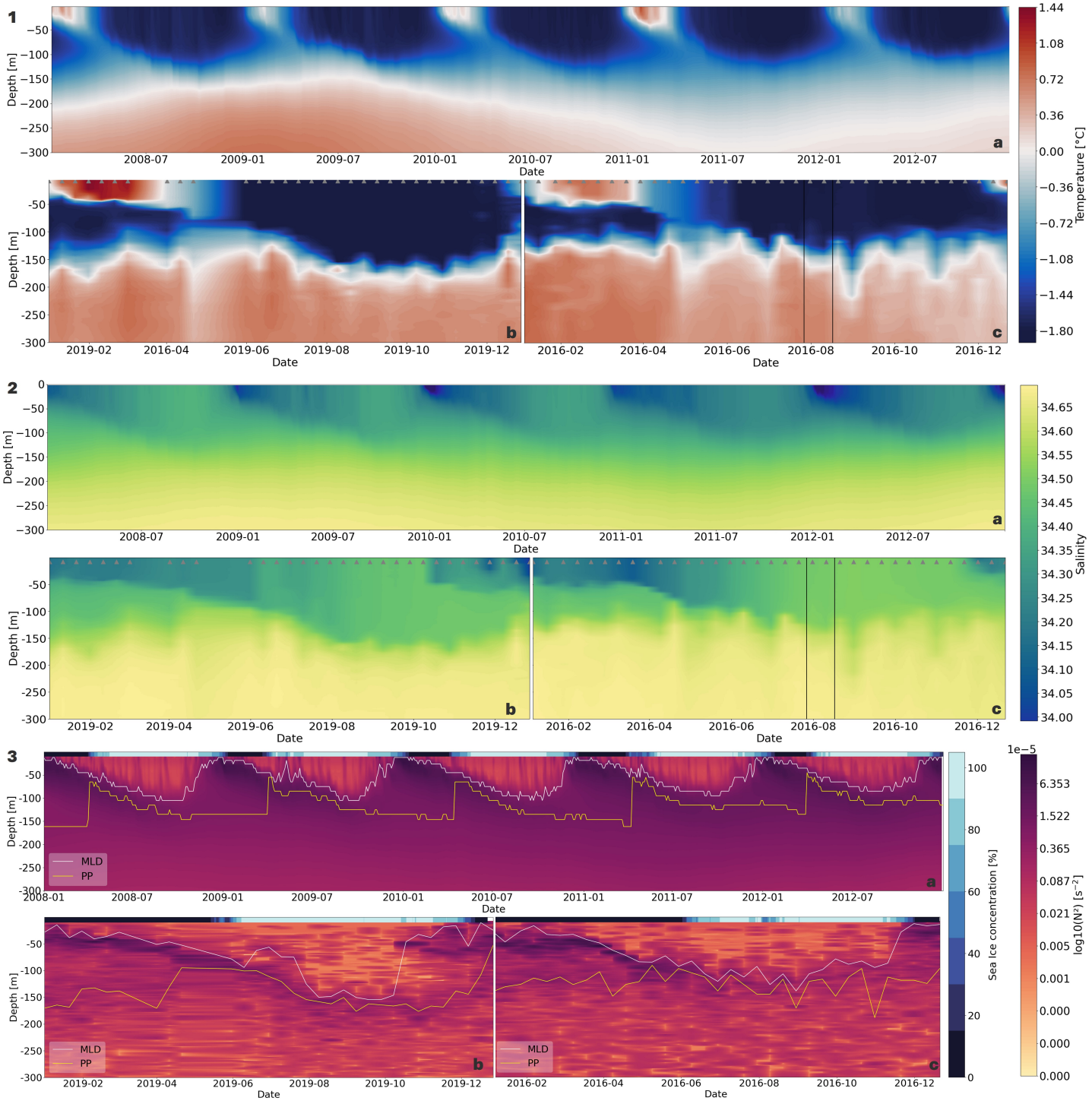

Figure 4: Upper ocean characteristics of all three sources. In **1** the temperature °C is shown for SOSE (a), 590538 Argo float for 2019 (b) and 5904471 Argo float for 2016(c). The grey triangles on the Argo figures (1 (a,b) 2(a,b)) indicate the date a profile was measured. The black vertical lines on the 2016 Argo figure(1c and 2c) show the timing of the polynya. Panel **2** shows the evolution of salinity, the layout is the same as in **1**. Panel **3** shows the evolution of $N^2[s^{-1}]$ and the SIC [%] on top. The mixed layer depth (MLD) is shown in white and the depth of the permanent pycnocline (PP) is in yellow. The layout remains the same as in panels **1** and **2**.

3.2 Oceanic Processes and Influences: Sea-Ice Dynamics, Heat Fluxes, and Wind Stress Curl.

3.2.1 Freshwater anomaly

The FWA exhibits a seasonal cycle, with a decline in FWA coinciding with the onset of sea-ice formation (Fig. 5). The absolute magnitudes for 2019 do not differ greatly; however, the observed pattern of a decline at the beginning of sea-ice formation is consistent with the SOSE throughout the years. Since the FWA is defined as the amount of sea-ice growth required to erode the halocline, the value decreases during the sea-ice growth and sea ice-covered season due to the release of brine, as less additional sea ice is required. In 2019 there is almost no change; 0.007 m between May and September, the winter period. The initial decline observed in 2019 is followed by a more stable period, which coincides with a reduction in the variability of the SIC. (Fig. 5, blue shading). During the sea-ice formation, the SIC was highly variable across the Maud Rise region and the initial decrease did not last until September, but only until July. In addition, the Argo float's location is not precisely known. This might have impacted the results. In the SOSE, 2011 has a high variability in SIC during sea-ice formation. Here the decrease is less steep until it drops in October. Nonetheless, there was a decrease in FWA between May and September of 0.18 m. Over the entire period, the change between May and September varies between 0.06 m in 2010 and 0.49 m in 2012.

Until summer the FWA increases again, coinciding with the observed freshening associated with sea-ice melt. In 2019, the minimum of additional sea ice needed is at 0.46 m. The minimum of the SOSE period was in 2008 with a value of 0.54 m. The inter-annual variability in the SOSE shows an increase in mean FWA until the end of 2011, from $0.90\,\mathrm{m} \pm 0.19\,\mathrm{m}$ in 2008 to $1.71\,\mathrm{m} \pm 0.11\,\mathrm{m}$, in 2011 FWA decreased to $1.39\,\mathrm{m} \pm 0.22\,\mathrm{m}$in 2012. This implicates that the upper ocean stability increased until 2012. The winter salinification decreased during the SOSE period, as described in 3.1, leading to a fresher upper ocean. Therefore, more brine input and hence more additional sea-ice growth would be required to erode the halocline. Further, the peaks in the FWA at the beginning of 2010 and 2012 coincide with a stronger freshwater signal than in the other years (Fig.4.2). The generally lower FWA in 2019 compared to SOSE is a result of a higher upper ocean salinity (Fig. 4.2). Another aspect that can impact the FWA is the duration of the sea-ice season. The SIC cycle in 2010 is shorter compared to other years, as the sea-ice formation began in April, while it has already started in March in the other. In addition, the sea ice was completely melted by the end of 2010. In the other years, the cycle lasted into the next year (Fig. 5). This could indicate overall less brine input throughout 2010 and could also be a result of the warmer surface layer compared to other years

Fig(4.a). For sea ice to form, the surface waters have to be cooled until freezing point. Starting from a higher temperature, this might take longer and lead to a delayed sea-ice formation. This in turn could lead to less brine input and an overall fresher upper ocean, resulting in a higher FWA. Similarly, the FWA in 2011 is the highest, which coincides with the low mixed layer salinity as described in section 3.1. The already fresher upper ocean and shorter sea-ice cycle, due to high variability in the beginning of the freezing period (Fig 5.a, blue shading), could have led to less salinification as mentioned above. The sea-ice cycle in 2012 is more similar to that observed in 2008 and 2009, with a stronger decrease in FWA between May and September, as previously mentioned, occurring alongside the seasonal cycle of upper ocean properties and the destabilisation of the upper ocean. The findings of this part indicate that the formation of sea ice has a negative impact on upper ocean stability, whereas the process of melting ice has a positive effect. The stability of the upper ocean is subject to fluctuations from year to year, influenced by a number of factors, including the salinity and temperature of the upper ocean and the duration of the sea-ice cycle.

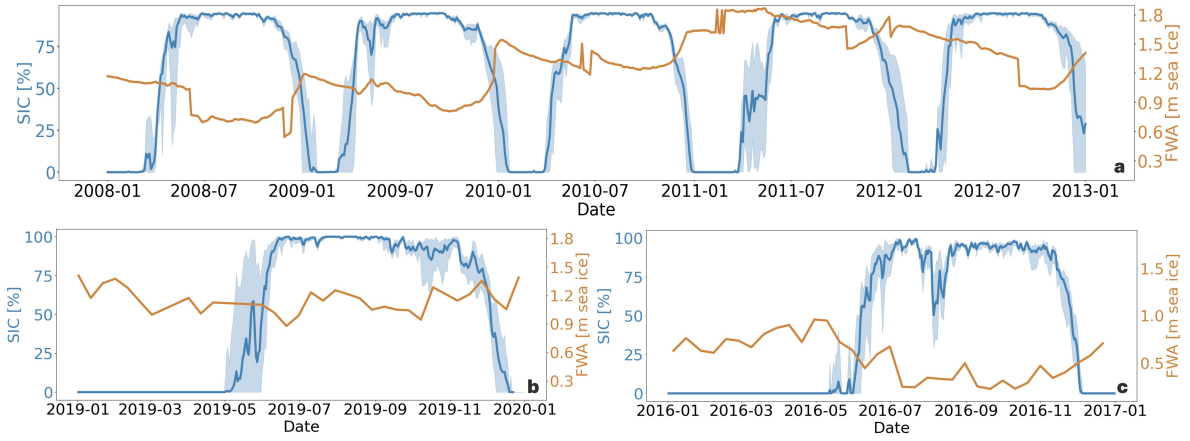

Figure 5: Freshwater anomaly (FWA) [m] and mean sea-ice concentration (SIC) [%] for the SOSE and both Argo floats. The SIC is depicted on the left y-axes in blue and the shading around the line are minimum and maximum values of the Maud Rise region for the specific dates. The upper panel (**a**) shows the results from the SOSE, in the lower left panel (**b**) the 590538 Argo float in 2019 and the lower right panel (**c**) the 5904471 Argo float in 2016.

3.2.2 Ocean heat content

As described in the methods section, I calculated the OHC for the upper ocean between 0 and 250 m and the depth layer encompassing the winter permanent pycnocline, 100 m − 200 m. The integrated OHC displays a slight seasonal cycle (Fig. 6). The cooling and brine release processes result in the densification of the mixed layer, which in turn leads to a deepening during the winter months (Fig. 4.1). This phenomenon subsequently decreases the OHC.

Between May and September 2019, OHC decreased by 6.8×10^8 J. The decrease in the SOSE is the lowest in 2018 with 1.7×10^7 J. In the following two years, the change OHC has become larger, reaching 9.86×10^7 J in 2010. After 2010, the decrease between May and September decreases again to 2.14×10^7 J in 2012. Overall, the change in OHC is generally lower in SOSE, this could be attributed to the coarser depth resolution. In December 2019, OHC increases again. This could, however, also be due to drift across a flank of Maud Rise. The seasonal cycle exhibits the highest values in March 2019 but for the SOSE between May and June. The lowest OHC occurs between August and November (Fig. 6), for both 2019 and SOSE. During this period, the mixed layer deepens, while the temperature beneath the sea ice remains consistently close to the freezing point of -1.8°C(Fig. 4.1).

For the depth interval covering the permanent pycnocline, $100 - 200$ m, the $\mathrm{OHC_P}$ peaks in March 2019, which coincides with a sudden vertical peak in CDW, but little change in the shallower ocean (Fig. 4.1.b), this might be due to the Argo changing its position. Throughout austral winter, until November, $\mathrm{OHC_P}$ decreases. The succeeding peak in $\mathrm{OHC_P}$ at the beginning of December does coincide with the melt of sea ice. However, since this cannot be observed in the integration over the $0 - 250$ m interval, it cannot be directly associated with the shift towards the sea ice-free period. It could rather be explained by the Argo float drifting away from the plateau of Maud Rise (Fig. 1) and the complex dynamics at the flanks that were described in the introduction.

The seasonal cycle can also be seen in the SOSE (Note: the y-axis covers a smaller range), although not as strong as in 2019. The highest $\mathrm{OHC_P}$ is observed between June and July in the SOSE, a pattern that is also evident in 2019, with the exception of the two peaks observed in March and December. In 2009 the $\mathrm{OHC_P}$ is slightly higher $\mathrm{OHC_P} = 1.065 \times 10^{11}$ J. The weaker change in winter in 2011 and 2012 can be seen in the difference between May and September. While the difference in 2010 was at 9.86×10^7 J it decreased to 2.52×10^7 J in 2011 and $2.15 \times 10^{7\,\mathrm{J}}$ in 2012. This might be due to the weaker vertical gradient in temperature in those years, as can be seen in Fig. 4.1.a. The difference across winter in 2019 5.801267×10^8 J. It can be observed that there is a slight seasonal cycle in the OHC integrated across the upper ocean and across the permanent pycnocline. The maximum value of the OHC is reached later across the permanent pycnocline than it is for the entire upper ocean.

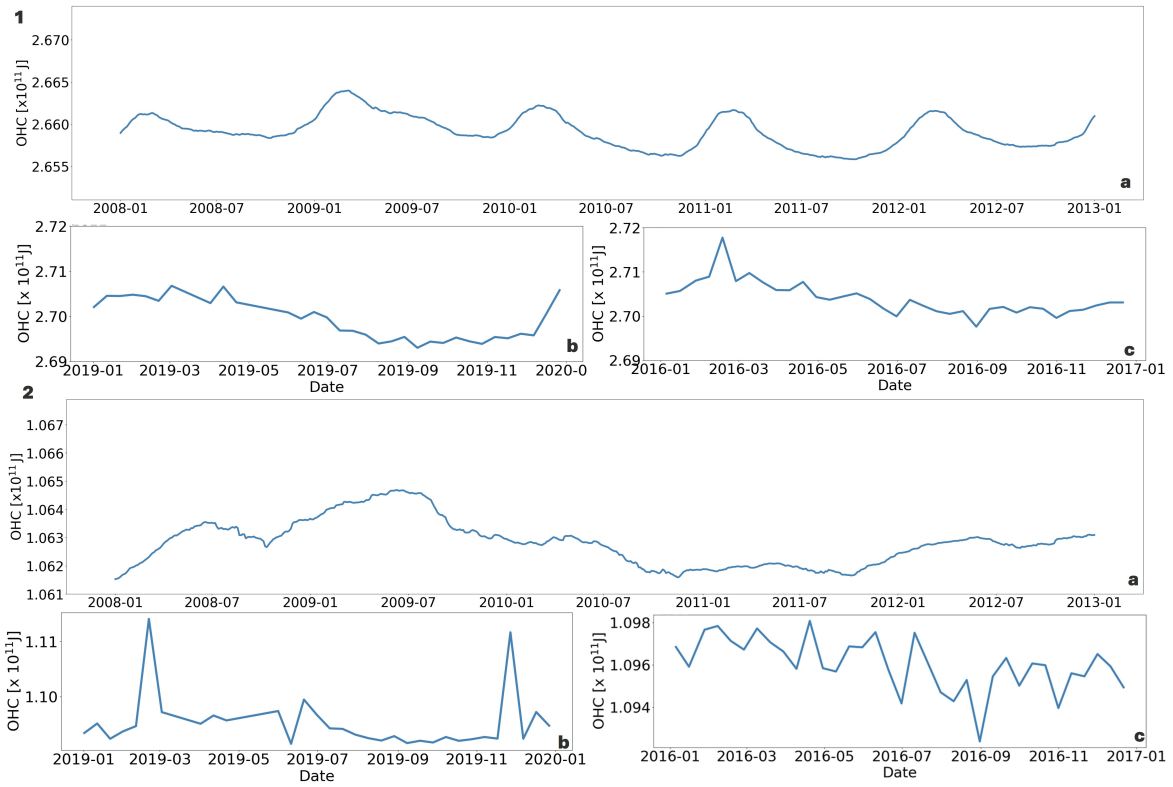

Figure 6: Panel **1** shows the integrated upper ocean heat content for the depth interval between 0 and 250 m. Panel **2** shows the ocean heat content for the depth interval across the winter permanent pycnocline between 100 m − 200 m (OHC_P). Both show the SOSE (**a**), the 590538 Argo float in 2019 (**b**) and the 5904471 Argo float in 2016.

3.2.3 Wind stress curl and upwelling

The wind stress curl does not show a strong seasonal pattern that could explain the shoaling of the permanent pycnocline around May (Fig. 7). The wind stress over Maud Rise is mainly negative, thus cyclonic. This cyclonic wind stress varies in intensity accompanied by storm events, for example at the end of September in 2019. The average wind stress curl lies at $-1.74 \times 10^{-7}\,\mathrm{N\,m^{-3}}$ for 2019 and for the entire $-2.44 \times 10^{-7}\,\mathrm{N\,m^{-3}}$ SOSE period. The associated upwelling induced by the wind stress is positive in the entire time frame. The maximum upwelling in 2019 was in October. Taking the 30-day rolling average the maximum upwelling was close to 10 m in October. In the entire period of the SOSE, the maximum was around 9 m in 2008 and slightly lower compared to 2019. In addition, the wind stress curl weakens slightly over the entire SOSE period (Fig.7.a). 2010 had the highest average wind stress curl. $-2.725 \times 10^{7}\,\mathrm{N\,m^{-3}} \pm 0.886 \times 10^{7}\,\mathrm{N\,m^{-3}}$, while it decreased until 2011 to $-2.318 \times 10^{7}\,\mathrm{N\,m^{-3}} \pm 0.932 \times 10^{7}\,\mathrm{N\,m^{-3}}$. The upwelling cannot be seen in the pycnocline depth directly (Fig.4.3). However, for example, in July 2019, following the upwelling event (Fig. 7), the OHC increased rapidly at the depth interval of the permanent pycnocline (Fig.

6), which could indicate a response to upwelling. This response is not visible in the overall OHC. For the results using the SOSE, no such observation can be made. Nevertheless, the strength of the permanent pycnocline (Fig. 3.a) appears to increase as the wind stress curl decreases when comparing data from different years. This observation does not necessarily imply that a weaker wind stress curl leads to a stronger permanent pycnocline.

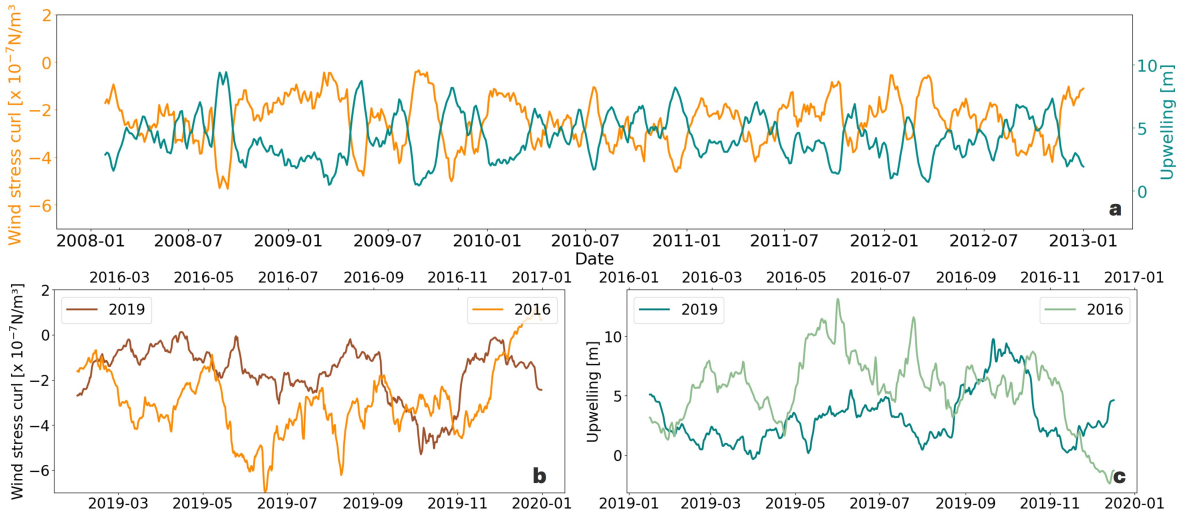

Figure 7: Panel **a** shows wind stress curl in orange and upwelling [m] for the SOSE period 2008 - 2012. Panel **b** shows wind stress curl [Nm^{-3}] for 2019 in brown and 2016 in orange. Panel **c** shows upwelling [m] for 2019 in dark green and 2016 in light green.

3.3 Comparison with a polynya year

Upper ocean properties

The structure of the upper ocean is the same as in 2019 and the SOSE period (Fig. 4), the winter mixed layer salinity in 2016 was overall higher compared to 2019 and the SOSE at 34.66 ± 0.04 (Fig. 4.2.c). Further, the depth of the permanent pycnocline is shallower at the beginning of the year, at around 140 m (Fig.4.3.c. The seasonal pycnocline is at approximately 50 m, where warm and fresh water lies above colder and saltier WW. The mixed layer deepening commences until the seasonal and permanent pycnocline merge in May at a depth of around 100 m. Similarly, to 2019 and the SOSE results, we observe a shoaling of the permanent pycnocline. The difference between January and May shows a shoaling of about 50 m. In 2019, the permanent pycnocline shoaled by over 70 m, in the SOSE the shoaling varies between 40 m and 80 m. However, there is no strong deepening after May until August as can be observed in the non-polynya years. In 2016, the permanent pycnocline only deepened by 30 m compared to 80 in 2019. There is a decrease at the end of August coinciding with the opening of the polynya, but otherwise, the permanent pycnocline remains at a depth shallower

than 150 m. The separation of the seasonal and permanent pycnocline also occurs later, only in November, compared to October as it does in 2019 and the SOSE. The strength of the permanent pycnocline in the polynya year does not increase as much as in 2019. However, the overall strength is of the same magnitude as the SOSE. The maximum can be observed in May, upon merging with the seasonal pycnocline, in accordance with 2019 and the SOSE. However, no clear cycle can be observed.

Freshwater anomaly

Similar to both other data sources, the FWA decreases with sea-ice growth. In addition, the amplitude of the change is more pronounced compared to the non-polynya year in 2019. The lowest values observed in 2016 were less than 0.2 m of additional sea-ice growth needed to erode the pycnocline. This is less than half compared to my previous results. In 2019, the lowest value was above 0.4 m and for the entire SOSE period it was 0.54 m. The winter salinification of the mixed layer was stronger compared to 2019 and the SOSE, as mentioned in the paragraph above. This decreased the FWA (Fig. 5.c) and thereby also the gradient in salinity between WW and CDW. The continuous increase in salinity could be explained by the opening of the polynya and the continuous refreezing of seawater, as the mixed layer temperature remained close to the freezing point (Fig. 4.1). This coincides with the lower stability (Fig.3) in 2016. The weak stability, N^2, and FWA values are a potential indicator that the water column was more vulnerable to entrainment or mixing across the pycnocline as well as overturning.

Ocean heat content

The OHC, on the other hand, shows a similar seasonal cycle. The depth interval between $0 - 250$ m shows a decrease until September and a slight increase until the end of the year. The decrease between May and September was lower compared to 2019 with 2.07×10^8 J. This is within the range of the decreases observed in the SOSE. The polynya did not seem to have a strong impact on the OHC. No strong signal can be observed during or after the polynya. Looking at the depth interval between $100\,\text{m} - 200\,\text{m}$ OHC_P does not show a seasonal cycle, compared to 2019. However, compared to the range of the SOSE, a decrease can be observed during winter. The decrease between May and September was 2.30×10^7 J, thus within the range of decreases in the SOSE. The evolution of OHC is more aligned with 2011 and 2012 in the SOSE data in terms of magnitude.

Wind stress curl and upwelling

The wind stress curl in 2016 is continuously negative throughout most of the year, just like in 2019 and the SOSE, but also stronger (Fig.7).a. The average wind stress curl was $-2.95 \times 10^{-7}\mathrm{Nm}^{-3}$. The upwelling over the 30-day rolling average was also higher compared to 2019 and the SOSE periods with a maximum of about 13 m in June (Fig. 7.c). However, at the end of the year, the curl becomes positive (Fig. 7.b). This would lead to downwelling (Fig. 7.c), but the analysed period is not long enough to determine in what way this affected the upper ocean characteristics and stratification. There are two especially strong winter storms in June and August. The storm in June and the associated divergence of the sea ice most likely contributed to the formation of the polynya at the end of July. During a quieter period between those two storms, the polynya closed up in mid-August. The second storm in August did not similarly impact the SIC, as the polynya closed up in August. Although, a slight decrease in SIC can be observed (Fig.4.3.c). Furthermore, the permanent pycnocline in 2016 was shallower than in 2019. The continuous increase in salinity could be due to the upwelling of salty water or continuous sea-ice formation, as mentioned before, and the associated brine rejection during sea-ice formation, due to the advection of sea ice caused by the wind stress curl.

4 Discussion

The seasonal evolution of the permanent pycnocline at Maud Rise is described in terms of its position and strength using measurements from two Argo floats and the SOSE. One of the Argo floats measured at Maud Rise during a polynya year, 2016. This was used to determine differences between non-polynya years, 2019, and the SOSE, and polynya years. The results between the Argo float non-polynya year, 2019, and SOSE non-polynya years are in agreement. This indicates that even point-in-time measurements made by singular floats allow us to understand changes in the ocean. The upper ocean properties, salinity, temperature and N^2, at Maud Rise undergo a strong seasonal cycle. The mixed layer deepens at the beginning of the year, while the permanent pycnocline shoals. The merging of the seasonal and permanent pycnoclines coincides with the onset of sea-ice formation between April and June, contingent on the timing of the sea-ice cycle. Upon merging with the seasonal pycnocline, the mixed layer continues to deepen until it reaches its maximum depth in September. During this process of deepening, the salinity of the water below the sea ice increases, while the temperature decreases until it reaches the freezing point of $-1.8\,^{\circ}\mathrm{C}$, forming WW. This temperature remains constant throughout the ice-covered period. At the end of the year, the melting of sea ice and

the warming of the mixed layer result in a decrease in the density of the mixed layer. This process results in the separation of the seasonal and permanent pycnoclines. The permanent pycnocline remains at the same depth level, where WW is separated from CDW and the seasonal pycnocline shoals to where the newly formed mixed layer is separated from the cold and salty WW. At the end of 2019, the permanent pycnocline also shallows, however, since the float drifted across one of the flanks this could also be due to its position encountering warmer water at the flanks. The annual process of merging between the seasonal and permanent pycnocline is not only observed regionally at Maud Rise but throughout the entire Weddell Sea (Libera et al., 2022). Further, the strength of the permanent pycnocline varies between the years. The difference between 2019 and the SOSE, can possibly be explained by the difference in depth resolution. The coarser depth resolution of SOSE, as mentioned earlier, can affect the ability to represent processes accurately. Nonetheless, there is also interannual variability between the years covered by the SOSE. In 2016 the permanent pycnocline was close to erosion, as can be seen by the low N^2 values (Fig.3). Other studies have found deep convection associated with the opening of the polynya (Campbell et al., 2019). In the data analysed here, this could not be observed. One reason could be that the Argo float was not located where the deep convection occurred. It is unlikely that the float was below the polynya opening, as it did not surface throughout the entire sea-ice-covered period.

The FWA showed that sea-ice formation destabilises the upper ocean. This is in accordance with previous studies (Wilson et al., 2019; Martinson and Wamser, 1990). A clear inter-annual change can be observed, especially in the SOSE data. In the SOSE it is visible that the depth of the permanent pycnocline is not constant on an inter-annual level but rather changes with upper ocean FWA. This variability in FWA is mainly driven by the mixed layer salinity. Salinity is the main determinant of ocean stratification in the polar regions (Pellichero et al., 2017). This affects the mixing between the mixed layer and lower water masses. Even though the permanent pycnocline acts as a barrier between the winter mixed layer and the underlying CDW, the strength of the stratification impacts the mixing of both water masses. In years with a lower FWA, meaning higher salinity, this gradient is weaker, and therefore the mixed layer is more vulnerable to heat entrainment. This heat prevents further sea-ice growth and thereby further brine input (Martinson, 1990; Wilson et al., 2019). In addition, in the years with a low FWA, the N^2 at the depth of the pycnocline was lower. Since the mixing coefficient κ is scaled with $N^2(\kappa = \frac{\Gamma\epsilon}{N^2})$ this indicates a weaker possibility of mixing and overturning. In 2016, however, the mixed layer salinity was higher and further increased over the course of the year. This high salinity led to a weaker gradient to CDW and coincided with a low FWA and low

values of N^2. Further, the high mixed layer salinity is in accordance with findings by Campbell et al. (2019), who analysed the linkages between offshore polynyas and climate anomalies in the Southern Hemisphere. They found that the mixed layer salinity was anomaly high compared to their Maud Rise climatology they calculated based on Argo floats, shipboard and instrumented seal measurements. Further, this agrees with (Klocker et al., 2022) who argue that the high stratification is a result of the density gradient across the permanent pycnocline which acts as the base of the mixed layer in winter. This may not be solely influenced by surface buoyancy fluxes but rather by the associated mixing processes. The increased salinity can, on one hand, be explained by the continuous formation of sea ice that is associated with polynyas. On the other hand, upwelling-induced entrainment of warm and salty is another potential explanation as the wind stress curl in 2016 was exceptionally high (Klocker et al., 2022) compared to 2019 and the SOSE. While FWA was lower in 2016 (Fig. 5) indicating a weakly stable upper ocean and a low strength of the permanent pycnocline, this entrainment cannot be inferred from either OHC or OHC_P. Campbell et al. (2019) found that the mixed layer temperature was increased during the months after the polynya opening. This increased temperature could be an indicator of upward entrainment of warm and salty CDW. The seasonal cycle of OHC_P was similarly weak in 2011, this can be attributed to a fresher mixed layer, which increases the stratification at the base and reduces the ability of upward entrainment. The overall OHC in 2016 and 2019 was higher than in SOSE, this could again be due to the coarser vertical resolution of the SOSE. In addition, 2019 shows a seasonal cycle in both OHC and OHC_P, which is comparable to the early years of the SOSE. In those years, the seasonal cycle of permanent pycnocline strength was more pronounced. The variations between the years indicate that both the strength and depth of the permanent pycnocline are affected by how strong the gradients between the winter mixed layer and CDW are, and thus the intensity of mixing between these water masses. This is, as mentioned before, in accordance with Klocker et al. (2022), who suggest that the layers of high stratification stem from sub-surface mixing processes rather than result from a vertical remapping of meridional surface density gradients as in classical theories(Luyten et al., 1983). The impact of WSC shows negative feedback. A high WSC features a weaker permanent pycnocline, which can be attributed to wind-driven upwelling of warmer and saltier subsurface water (Kurtakoti et al., 2018; Cheon et al., 2015; Martinson et al., 1981). The depth of the permanent pycnocline is then again dependent on background stratification, and the intensity of mixing processes is likely to be dependent on the strength of stratification and WSC. However, WSC, as well as SIC have been averaged over the previously defined Maud Rise box. Thus, there is some location bias when compared to

results from point-in-time measurements, such as Argo floats. Next to that, the coarser depth resolution of the SOSE data has most likely influenced the magnitude of changes or overall strength compared to Argo results. Additional uncertainties could have impacted this analysis, such as the uncertainty of accurately representing the temperature at a depth of about 100 m (Mazloff and for Atmospheric Research Staff , Eds). In addition, there are also uncertainties in the Argo data, next to the accuracy of the measurement instruments, as mentioned in the data section. The coarse temporal and spatial resolution of the Argo float measurements adds additional uncertainty in terms of changes in ocean characteristics that are mainly due to the change of location. In addition, the spatial interpolation during the sea-ice-covered period can give an additional location bias. This is further amplified by the spatial inhomogeneity at Maud Rise (De Steur et al., 2007) and the ocean dynamics in terms of the Taylor Cap and warm water flanks (Muench et al., 2001).

Even though these biases might have an influence on this analysis, the results that can be observed show that there is a relationship between background stratification and destabilising forces, such as brine rejection or wind stress, and the characteristics of the permanent pycnocline. Thus, the interplay between the interactions of ice-sea fluxes, heat and salt mixing or diffusion and wind stress-induced upwelling are likely to determine these characteristics.

5 First thoughts on future work

5.1 Interannual climate variability

This study shows the seasonal evolution of the permanent pycnocline has distinct interannual differences. Even though the general evolution follows a similar pattern, the stability of the permanent pycnocline and its vertical position differ from year to year. Therefore, understanding what conditions impact general upper ocean properties and might lead to preconditioning of a shallow or weak is necessary to understand the overall impacts on the permanent pycnocline. Atmospheric indices such as the Southern Annular Mode (SAM) or El Niño Southern Oscillation (ENSO) have been shown to impact the ocean in a variety of ways, especially in terms of wind forcing or precipitation rates (Gordon et al., 2007). Therefore, it could be of interest to analyse whether there is any connection between the phases of the SAM and interannual differences in background stratification over a longer timescale as seen in the results of the SOSE.

5.2 Thermobaric processes and densification

Multiple studies have shown the importance of non-linear effects of the equation of state when it comes to the formation and transformation of water masses (Groeskamp et al., 2016). The seasonal evolution of the permanent pycnocline is subject to various dynamic processes including mixing that influence its stability and depth. Future research could investigate the potential impacts of thermobaricity and cabbeling on this seasonal evolution. Thermobaricity, the variation of water density with both temperature and pressure, and cabbeling, the non-linear interaction between temperature and salinity leading to denser water masses, represent two intricate mechanisms that can significantly affect the stability of the pycnocline. While thermobaricity amplifies density gradients with depth due to the compressibility of seawater, cabbeling can induce local density anomalies that may contribute to the reshaping of density profiles within the water column. This is especially interesting, as there is a small layer of cold and fresh water in between warmer and saltier waters, while the mixed layer deepens between March and May (Appendix: A). This coincides with the T-S-space where WW is connected to deep water, and intermediate according to Evans et al. (2018). TThe study found that deep water cools and freshens due to mixing with WW. This occurs as a result of subsurface mixing, which occurs upon densification of WW as a result of brine rejection during sea-ice formation. In addition, thermobaricity has also been shown to play an important role in triggering convection events, specifically at Maud Rise (Akitomo, 2006). Thus, analysing the impact of non-linearities on the seasonal evolution of the upper ocean and its potential impact on the permanent pycnocline could help us understand more about its formation and evolution.

6 Conclusion

In this study, I analysed Argo float data during a polynya year and compared my findings to measurements of another Argo float that measured during a non-polynya year, as well as the SOSE. The overall seasonal evolution of the upper ocean characteristics follows the same seasonal cycle. There are, however, interannual differences in temperature and salinity stratification that impact the seasonal evolution of strength and depth of the permanent pycnocline. I identified a shoaling of the pycnocline in austral autumn right before merging with the seasonal pycnocline. Further, the results show that freshwater forcing governs changes in the strength and depth of the permanent pycnocline. Background stratification, especially salinity, meaning the upper ocean freshwater content in that specific year, affects the gradient

of the upper ocean salt stratification and the strength of the permanent pycnocline impacts the ability to mix with deeper water masses and thereby the overall stability of the water column. The results show that the seasonal evolution of depth and strength is more pronounced in a non-polynya year. In 2016, the polynya year, the change in depth was less pronounced and could also have been influenced by the drift of the Argo float. Further, the strength of the permanent pycnocline fluctuated more in 2016 and did not seem to follow a distinct seasonal cycle, as it did in the non-polynya years. Heightened wind stress acted upon the already weaker stratification and has been invoked as one of the aspects that lead to the formation of the polynya (Campbell et al., 2019). In general, wind stress can further affect the gradient between cold and salty upper winter water and warm and salty sub-surface water, by inducing upwelling. Moving forward, it would be interesting to see if the inter-annual variabilities can be connected to climate variability, such as in the SAM. It would also be interesting to compare further years to determine how the upper ocean salinity is changing and how years with low sea-ice extent in the entire Southern Hemisphere compare to previous years. This would help to unravel how preconditioning of the upper ocean can impact the permanent pycnocline and how non-linearities in the mixing process can impact the permanent pycnocline.

A Appendix

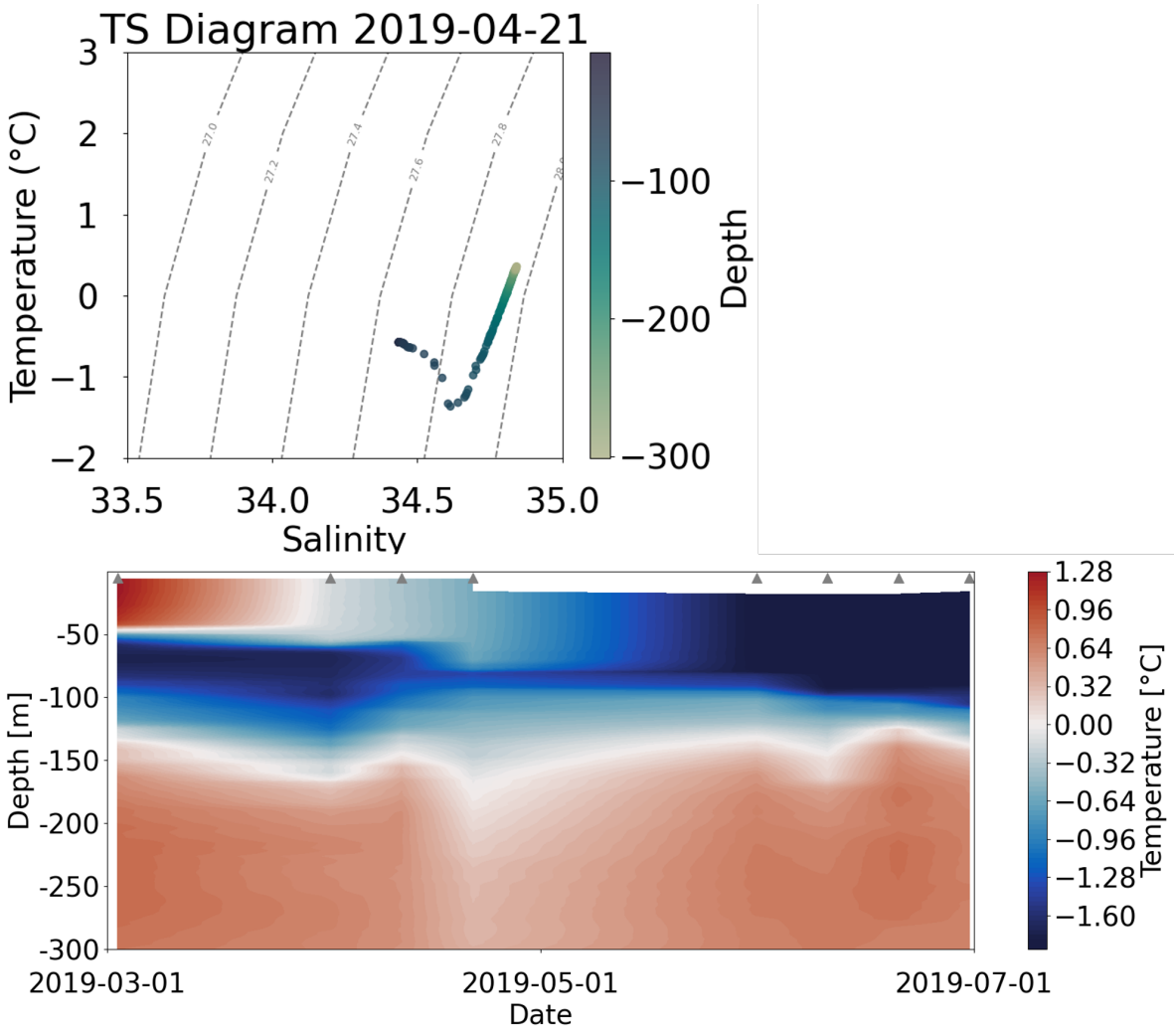

Appendix A: The upper TS-Diagram shows the temperature and salinity for April 21 2019, the contour plot below shows the evolution of temperature for 2019 for austral autumn, highlighting the cold anomaly at around 100 m.

Acknowledgements

I want to thank my supervisors Prof. Dr. Eleanor Frajka-Williams and Prof. Dr. Alberto Naveira Garabato as well as the entire second floor of the Institute of Oceanography at Universität Hamburg for their steady support and all the valuable discussions we have had. Last but not least I want to thank Zachary Mühlenweg for his support and proofreading.

These data were collected and made freely available by the International Argo Program and the national programs that contribute to it. (https://argo.ucsd.edu, https://www.ocean-ops.org). The Argo Program is part of the Global Ocean Observing System.
NCEP-NCAR Reanalysis 1 data provided by the NOAA PSL, Boulder, Colorado, USA, from their website at https://psl.noaa.gov.
Computational resources for the SOSE were provided by NSF XSEDE resource grant OCE130007. The SOSE solution for the years 2008–2012, denoted iteration 105, is available from sose.ucsd.edu. The observations used for model validation are available from the NOAA National Ocean Data Center (http://www.nodc.noaa.gov/).

Bibliography

Abernathey, R. P., Cerovecki, I., Holland, P. R., Newsom, E., Mazloff, M., and Talley, L. D. (2016). Water-mass transformation by sea ice in the upper branch of the southern ocean overturning. *Nature Geoscience*, 9(8):596–601.

Akitomo, K. (2006). Thermobaric deep convection, baroclinic instability, and their roles in vertical heat transport around maud rise in the weddell sea. *Journal of Geophysical Research: Oceans*, 111(C9).

Argo (n.d.). How do floats work. Accessed: December 20, 2023.

Beckmann, A., Timmermann, R., Pereira, A. F., and Mohn, C. (2001). The effect of flow at maud rise on the sea-ice cover–numerical experiments. *Ocean Dynamics*, 52:11–25.

Brandt, A., Bathmann, U., Brix, S., Cisewski, B., Flores, H., Göcke, C., Janussen, D., Krägefsky, S., Kruse, S., Leach, H., Linse, K., Pakhomov, E., Peeken, I., Riehl, T., Sauter, E., Sachs, O., Schüller, M., Schrödl, M., Schwabe, E., Strass, V., van Franeker, J., and Wilmsen, E. (2011). Maud rise – a snapshot through the water column. *Deep Sea Research Part II: Topical Studies in Oceanography*, 58(19):1962–1982. Southern Ocean Biodiversity — From Pelagic Processes to Deep-Sea Response.

Campbell, E. C., Wilson, E. A., Moore, G., Riser, S. C., Brayton, C. E., Mazloff, M. R., and Talley, L. D. (2019). Antarctic offshore polynyas linked to southern hemisphere climate anomalies. *Nature*, 570(7761):319–325.

Carmack, E. C. (2007). The alpha/beta ocean distinction: A perspective on freshwater fluxes, convection, nutrients and productivity in high-latitude seas. *Deep Sea Research Part II: Topical Studies in Oceanography*, 54(23-26):2578–2598.

Cheon, W. G., Lee, S.-K., Gordon, A. L., Liu, Y., Cho, C.-B., and Park, J. J. (2015). Replicating the 1970s' weddell polynya using a coupled ocean-sea ice model with reanalysis surface flux fields. *Geophysical Research Letters*, 42(13):5411–5418.

Copernicus Climate Change Service (C3S) (2020). Sea ice concentration daily gridded data from 1978 to present derived from satellite observations. Copernicus Climate Change Service (C3S) Climate Data Store (CDS). Accessed on 30-01-2024.

De Steur, L., Holland, D., Muench, R., and Mcphee, M. G. (2007). The warm-water "halo" around maud rise: Properties, dynamics and impact. *Deep Sea Research Part I: Oceanographic Research Papers*, 54(6):871–896.

DeVries, T. and Primeau, F. (2011). Dynamically and observationally constrained estimates of water-mass distributions and ages in the global ocean. *Journal of Physical Oceanography*, 41(12):2381–2401.

EUMETSAT Ocean and Sea Ice Satellite Application Facility (2023). OSI SAF Global Sea Ice Concentration (AMSR-2). Data extracted from copernicus.eu: ([2016,2019) ([62°S − 68°S; 0°E − 10°E],) accessed [30-01-2024]. OSI-408-a.

Evans, D. G., Zika, J. D., Naveira Garabato, A. C., and Nurser, A. G. (2018). The cold transit of southern ocean upwelling. *Geophysical Research Letters*, 45(24):13–386.

Gill, A. E. (1982). *Atmosphere-ocean dynamics*, volume 30. Academic press.

Gnanadesikan, A. (1999). A simple predictive model for the structure of the oceanic pycnocline. *Science*, 283(5410):2077–2079.

Gordon, A. L. (1991). Two stable modes of southern ocean winter stratification. In *Elsevier Oceanography Series*, volume 57, pages 17–35. Elsevier.

Gordon, A. L., Visbeck, M., and Comiso, J. C. (2007). A possible link between the weddell polynya and the southern annular mode. *Journal of Climate*, 20(11):2558–2571.

Gregor, L., Ryan-Keogh, T. J., Nicholson, S.-A., du Plessis, M.and Giddy, I., and Swart, S. s. (2019). Glidertools: A python toolbox for processing underwater glider data. *Journal of Geophysical Research: Oceans*, (6):1–13.

Groeskamp, S., Abernathey, R. P., and Klocker, A. (2016). Water mass transformation by cabbeling and thermobaricity. *Geophysical Research Letters*, 43(20):10–835.

Handcock, M. S. and Raphael, M. N. (2020). Modeling the annual cycle of daily antarctic sea ice extent. *The Cryosphere*, 14(7):2159–2172.

Hoyer, S. and Hamman, J. (2017). xarray: N-D labeled arrays and datasets in Python. *Journal of Open Research Software*, 5(1).

Kalnay, E., Kanamitsu, M., Kistler, R., Collins, W., Deaven, D., Gandin, L., Iredell, M., Saha, S., White, G., Woollen, J., Zhu, Y., Leetmaa, A., Reynolds, R., Chelliah, M., Ebisuzaki, W., Higgins, W., Janowiak, J., Mo, K. C., Ropelewski, C., Wang, J., Jenne, R., and Joseph, D. (1996). The NCEP/NCAR 40-year reanalysis project. *Bulletin of the American Meteorological Society*, 77:437–470.

Klatt, O., Boebel, O., and Fahrbach, E. (2007). A profiling float's sense of ice. *Journal of Atmospheric and Oceanic Technology*, 24(7):1301–1308.

Klocker, A., Garabato, A. N., Roquet, F., de Lavergne, C., and Rintoul, S. (2022). Generation of the southern ocean pycnocline by sea ice-ocean interactions. *Authorea Preprints*.

Kurtakoti, P., Veneziani, M., Stössel, A., and Weijer, W. (2018). Preconditioning and formation of maud rise polynyas in a high-resolution earth system model. *Journal of Climate*, 31(23):9659–9678.

Libera, S., Hobbs, W., Klocker, A., Meyer, A., and Matear, R. (2022). Ocean-sea ice processes and their role in multi-month predictability of antarctic sea ice. *Geophysical Research Letters*, 49(8):e2021GL097047.

Luyten, J., Pedlosky, J., and Stommel, H. (1983). The ventilated thermocline. *Journal of Physical Oceanography*, 13(2):292–309.

Martinson, D. G. (1990). Evolution of the southern ocean winter mixed layer and sea ice: Open ocean deepwater formation and ventilation. *Journal of Geophysical Research: Oceans*, 95(C7):11641–11654.

Martinson, D. G. and Iannuzzi, R. A. (1998). Antarctic ocean-ice interaction: Implications from ocean bulk property distributions in the weddell gyre. *Antarctic sea ice: physical processes, interactions and variability*, 74:243–271.

Martinson, D. G., Killworth, P. D., and Gordon, A. L. (1981). A convective model for the weddell polynya. *Journal of Physical Oceanography*, 11(4):466–488.

Martinson, D. G. and Wamser, C. (1990). Ice drift and momentum exchange in winter antarctic pack ice. *Journal of Geophysical Research: Oceans*, 95(C2):1741–1755.

Mazloff, M. and for Atmospheric Research Staff (Eds), N. C. (2022). The Climate Data Guide: Southern Ocean State Estimate (SOSE). Last modified 2022-09-09. Retrieved from `https://climatedataguide.ucar.edu/climate-data/southern-ocean-state-estimate-sose` on 2024-04-25.

McDougall, T. and Barker, P. (2011). Getting started with teos-10 and the gibbs seawater (gsw) oceanographic toolbox. *Journal of Geophysical Research: Oceans*, page 28pp.

Muench, R., Morison, J., Padman, L., Martinson, D., Schlosser, P., Huber, B., and Hohmann, R. (2001). Maud rise revisited. *Journal of Geophysical Research: Oceans*, 106(C2):2423–2440.

Pedro, J., Martin, T., Steig, E., Jochum, M., Park, W., and Rasmussen, S. (2016). Southern ocean deep convection as a driver of antarctic warming events. *Geophysical Research Letters*, 43(5):2192–2199.

Pellichero, V., Sallée, J.-B., Chapman, C. C., and Downes, S. M. (2018). The southern ocean meridional overturning in the sea-ice sector is driven by freshwater fluxes. *Nature communications*, 9(1):1789.

Pellichero, V., Sallée, J.-B., Schmidtko, S., Roquet, F., and Charrassin, J.-B. (2017). The ocean mixed layer under southern ocean sea-ice: Seasonal cycle and forcing. *Journal of Geophysical Research: Oceans*, 122(2):1608–1633.

Resplandy, L., Séférian, R., and Bopp, L. (2015). Natural variability of co2 and o2 fluxes: What can we learn from centuries-long climate models simulations? *Journal of Geophysical Research: Oceans*, 120(1):384–404.

Samelson, R. and Vallis, G. K. (1997). Large-scale circulation with small diapycnal diffusion: The two-thermocline limit. *Journal of Marine Research*, 55(2):223–275.

Scripps Institution of Oceanography (2016). Biogeochemical Southern Ocean State Estimate Solution. Copernicus Climate Change Service (C3S) Climate Data Store (CDS). Ocean State Estimation at Scripps Institution of Oceanography.

Verdy, A. and Mazloff, M. R. (2017). A data assimilating model for estimating s outhern o cean biogeochemistry. *Journal of Geophysical Research: Oceans*, 122(9):6968–6988.

Wilson, E. A., Riser, S. C., Campbell, E. C., and Wong, A. P. (2019). Winter upper-ocean stability and ice–ocean feedbacks in the sea ice–covered southern ocean. *Journal of Physical Oceanography*, 49(4):1099–1117.

Wong, A. P. and Riser, S. C. (2011). Profiling float observations of the upper ocean under sea ice off the wilkes land coast of antarctica. *Journal of Physical Oceanography*, 41(6):1102–1115.

Declaration

Hiermit versichere ich an Eides statt, dass ich die vorliegende Arbeit im Studiengang M.Sc. Ocean and Climate Physics selbstständig verfasst und keine anderen als die angegebenen Hilfsmittel – insbesondere keine im Quellenverzeichnis nicht benannten Internet-Quellen – benutzt habe. Alle Stellen, die wörtlich oder sinngemäß aus Veröffentlichungen entnommen wurden, sind als solche kenntlich gemacht. Ich versichere weiterhin, dass ich die Arbeit vorher nicht in einem anderen Prüfungsverfahren eingereicht habe und dass die gedruckte der elektronischen Fassung entspricht.

Einer Veröffentlichung der vorliegenden Arbeit in der zuständigen Fachbibliothek des Fachbereichs stimme ich zu.

Hamburg, April 29, 2024 Viktoria Nikolaus